

Article

Investigation of Novel Transition Metal Loaded Hydrochar Catalyst Synthesized from Waste Biomass (Rice Husk) and Its Application in Biodiesel Production Using Waste Cooking Oil (WCO)

Laraib Aamir Khan ¹, Rabia Liaquat ^{1,*}, Mohammed Aman ², Mohammad Kanan ² , Muhammad Saleem ³ , Asif Hussain khoja ¹ , Ali Bahadar ⁴  and Waqar Ul Habib Khan ¹ 

- ¹ U.S-Pakistan Centre for Advanced Studies in Energy (USPCAS-E), National University of Sciences & Technology (NUST), Sector H-12, Islamabad 44000, Pakistan; laraibaamir786@gmail.com (L.A.K.); asif@uspcase.nust.edu.pk (A.H.k.); waqarmahsud18@gmail.com (W.U.H.K.)
- ² Department of Industrial Engineering, College of Engineering, University of Business and Technology, Jeddah 21448, Saudi Arabia; m.aman@ubt.edu.sa (M.A.); m.kanan@ubt.edu.sa (M.K.)
- ³ Department of Industrial Engineering, King Abdulaziz University, Rabigh 21911, Saudi Arabia
- ⁴ Department of Chemical and Materials Engineering, King Abdulaziz University, Rabigh 21911, Saudi Arabia; absali@kau.edu.sa
- * Correspondence: rabia@uspcase.nust.edu.pk

Abstract: The decarbonization of transportation plays a crucial role in mitigating climate change, and biodiesel has emerged as a promising solution due to its renewable and eco-friendly nature. However, in order to maintain the momentum of the “green trend” and ensure energy security, an ecologically friendly pathway is important to produce efficient biodiesel. In this work, activated carbon (AC) obtained from rice husk (RH) is hydrothermally prepared and modified through cobalt transition metal for catalyst support for the transesterification process. The physicochemical characteristics of the synthesized catalysts are examined using XRD, FTIR, SEM and EDS, TGA, and BET, while the produced biodiesel is also characterized using Gas Chromatography and Mass Spectroscopy (GC-MS). To optimize the transesterification process, Fatty Acid Methyl Esters (FAME) are produced by the conversion of waste cooking oil. Response Surface Methodology (RSM) is used to validate temperature (75 °C), the methanol-to-oil molar ratio (1:9), catalyst weight percentage (2 wt.%), and retention time (52.5 min). The highest conversion rate of waste cooking oil (WCO) to biodiesel was recorded at 96.3% and tested as per American Society for Testing and Materials (ASTM) standards. Based on the results, it is clear that cobalt-loaded rice husk-based green catalyst (RHAC-Co) enhanced catalytic activity and yield for biodiesel production. Further research should focus on engine performance evaluation and scaling up of the catalyst by optimizing it for the industrial scale.

Keywords: activated carbon; heterogeneous catalyst; hydrothermal carbonization; transesterification; biodiesel; response surface methodology (RSM)



Citation: Khan, L.A.; Liaquat, R.; Aman, M.; Kanan, M.; Saleem, M.; khoja, A.H.; Bahadar, A.; Khan, W.U.H. Investigation of Novel Transition Metal Loaded Hydrochar Catalyst Synthesized from Waste Biomass (Rice Husk) and Its Application in Biodiesel Production Using Waste Cooking Oil (WCO). *Sustainability* **2024**, *16*, 7275. <https://doi.org/10.3390/su16177275>

Academic Editors: Antonella Angelini and Carlo Pastore

Received: 10 July 2024

Revised: 14 August 2024

Accepted: 21 August 2024

Published: 23 August 2024



Copyright: © 2024 by the authors. Licensee MDPI, Basel, Switzerland. This article is an open access article distributed under the terms and conditions of the Creative Commons Attribution (CC BY) license (<https://creativecommons.org/licenses/by/4.0/>).

1. Introduction

Global transportation sector emissions from non-renewable fuels have risen alarmingly worldwide, contributing to global warming and climate change [1]. To avoid the threat of climate change, in the year 2016, the Paris Agreement was introduced. The core long-term goals of this agreement were to keep the increase in global average temperature well below 2 °C above the pre-industrial levels, and secondly, to pursue efforts to limit the rise to 1.5 °C, as subsequently, this would considerably lessen the dangers and effects of climate change in the second half of the century [2]; significant actions should be taken to reduce the transportation demand and decarbonize the remaining emissions. Also, fossil fuels, including crude oil and coal, have long been known as the world’s principal sources of

energy for transportation, industrial use, and home use. Eventually, these energy sources tend to run out and have environmental problems [3]. Their increased depletion, the rise in oil costs, and environmental concerns have made the production of biodiesel a crucial topic of research [4], being a renewable and sustainable fuel, and this is why the alternative to diesel is required to meet the global demand.

Biodiesel is the most promising candidate among biofuels produced through the transesterification reaction of oil with alcohol in the presence of a catalyst [5], which is gaining a lot of interest nowadays [3]. Biodiesel is sulfur-free, non-toxic, and biodegradable, with far greater lubricating capabilities than petroleum diesel [6]. Besides petroleum diesel, biodiesel as an alternative has a lower carbon footprint while running existing diesel engines with no significant modification being necessary [7], making it a cost-effective and easily implementable solution for decarbonizing transportation derived from sources other than fossil fuels [6]. When compared to conventional diesel fuel, one of the primary obstacles to the commercial use of biodiesel is its higher cost of production [8]. A substantial amount of the operational costs of the biodiesel synthesis process are dependent on the feedstock that is used, therefore choosing a cost-effective feedstock can achieve significant economic impact on the industry [9,10]. They provide a way to gradually reduce emissions for the current vehicle fleet and sectors such as freight [11], maritime, and air transportation [12], and are currently vital and practical solutions in addressing climate change [13], sustainable development, and better management of greenhouse gases [14,15]. Biodiesel produced from edible oils is derived from plant-based sources, e.g., corn, sunflower, soya bean, cottonseed, coconut, groundnut, rapeseed, palm, castor, and soybeans, which are first-generation feedstocks [16]. They have the potential to produce biodiesel, which is known as first-generation biodiesel, but they are costly currently at large industrial scale and spark the concern of food shortage for human consumption for fuel. This scenario creates a great challenge in keeping the production cost at a comfortable margin [9]. Researchers have been provoked to generate second-generation biodiesel from sustainable non-edible sources such as non-edible crops (vegetable and algal oil), animal fat, and oil waste (waste animal oil and waste cooking oil), which are known as second-generation feedstocks. For industrial-scale biodiesel production, therefore, the utilization of oil waste sources (WCO and animal fats) is growing, which makes the entire process of production more sustainable [17].

Waste cooking oil (WCO) is an edible oil that is used in restaurants and hotels but is no longer in use. Its improper disposal harms water quality and fish populations, other aquatic life, and local communities [18]. 16.5 million tons of WCO are generated worldwide by the food industry and kitchens, and these materials are either dumped in landfills with other municipal garbage or discharged into the sewage system [19]. As a feedstock, it is employed for making biodiesel because of its three main advantages: economic, environmental sustainability, and waste management [20,21]. WCO can be catalytically cracked using a variety of catalysts that include metal oxides, zeolites, magnetic nanoparticles, silica gels, resins, and activated carbon [3]. The efficiency and effectiveness of the process can be influenced by the choice of catalyst used [22,23]. In recent years, heterogeneous catalysts have come into focus as an alternative option for producing biodiesel [24], because homogeneous catalysts have limitations [25]. Heterogeneous catalysts have several advantages that include easy product separation, reusability, and no negative environmental impact during production [3].

Using agricultural waste such as rice husk (RH), which is a readily available and underutilized by-product of rice milling, as a catalyst can lower the cost of biodiesel production in comparison to conventional catalysts, as it can eliminate the costs and their environmental impact and is applicable in a wide range of applications [26]. Activated carbon (AC) can be prepared from a variety of materials such as agricultural waste because they are rich in carbon and have high amorphous content, as such, it is an intriguing and affordable option due to their low cost and environmental benefits [27].

Hydrothermal carbonization (HTC) is a thermochemical process used as an initial step in producing catalysts that involve the heating of the materials to autogenous pressures to form char. Unlike pyrolysis [28] and other traditional carbonization techniques, this procedure doesn't require any such precautions, requires no biomass pre-drying, and runs at 200–300 °C [29]. Lower operating temperatures in HTC preserve nitrogen, sulfur, and oxygen concentrations, making it an attractive option for processing biomass with a high moisture content that would otherwise necessitate a great deal of energy to dry. Approximately 100% of RH may be converted into hydrochar (HC) [30,31]. It is chemically activated to produce AC, aiding in the catalytic cracking of WCO [27], and is used as a support owing to its amorphous characteristics, large surface area, highly interior pore structure, and modifiable surface chemistry [27,32]. As compared to an HZSM-5 catalyst, studies demonstrate that AC results in higher WCO conversion and liquid product yield [33]. When it comes to loading catalysts onto AC, transition metals are considered a cost-effective and non-toxic alternative to noble metal catalysts offering basic or acidic sites for chemical reactions, and their active phase is affixed to a highly porous substrate with a large surface area to facilitate catalysis [34]. Transition metal like cobalt (Co) is known to boost the properties of catalysts, and is relatively inexpensive, unlike other transition metals such as rhodium and palladium which have significant catalytic reactivity [35]. Research conducted by Thangadurai et.al [36] also discovered that AC combined with metal oxides has the potential to catalytically crack and produce biofuels. Apart from thermochemical procedures, such as pyrolysis and HTC, lipase enzymes provide an enzymatic approach to produce biodiesel. Under favorable circumstances, lipase promotes the transesterification of triglycerides, resulting in high-purity biodiesel with less byproducts. Large-scale applications, however, may be constrained by the requirement for the immobilization of enzymes for stability. Despite this, the selectivity, reduced energy requirements, and potential to process high-FFA oils without prior or pre-treatment make enzymatic techniques attractive [37]. Lipase enzymes offer an environmentally friendly [38], sustainable substitute, whereas metal-loaded catalysts and HTC offer scalable solutions.

Several process parameters play a crucial role in optimizing and stabilizing biodiesel production yield. Studies have shown that using an RSM can significantly improve the production of biofuels [39]. This approach involves analyzing the interactions between different process parameters and identifying the optimal combination for maximum yield. Studying the relationship between the inputs and outputs helps to identify the ideal process conditions making the production process efficient. However, this approach can lead to higher production yields and improve the economic viability of biofuel production [7,40]. A novel approach of cobalt immobilization on activated carbon support material for transesterification of WCO was studied in this research. According to the authors' information, no comprehensive study has been reported so far on the synthesis of an economical and environmentally beneficial catalyst by using a transition metal on rice husk-derived activated hydrochar through hydrothermal carbonization (HTC) for biodiesel production.

The focus of this study is to find a new way to convert used WCO into biodiesel by developing novel heterogeneous rice husk-derived cobalt-loaded activated carbon (RHAC-Co) catalysts. The catalyst is then characterized using Fourier Transform Infrared Spectroscopy (FTIR), X-ray diffraction (XRD), Brunauer Emmett and Teller (BET), Thermogravimetric Analysis (TGA), Scanning Electron Microscopy (SEM), and Energy Dispersive Spectroscopy (EDS) characterizations. Complete characterization of the produced biodiesel using (RHAC-Co) catalysts was carried out to prove its feasibility as fuel. Furthermore, the relationship between independent process parameters and optimum conditions of biodiesel yield was studied via RSM. The percentage yield of biodiesel (YBD) is affected by input variables and that effect was studied using the central composite design (CCD).

2. Materials and Methods

2.1. Material Collection

Waste cooking oil (WCO) was collected from the Concordia Cafe (C2) at the National University of Sciences and Technology (NUST), Islamabad, Pakistan. Rice husk was obtained from rice fields in a village located near Rawalpindi, Pakistan. Sulfuric acid, methanol, cobalt nitrate hexahydrate $\text{Co}(\text{NH}_3)_2 \cdot 6\text{H}_2\text{O}$, deionized and distilled water from Sigma Aldrich (St. Louis, MO, USA) with a purity of 99% were used in all experiments. The physiochemical properties of Waste cooking oil (WCO) are reported in Table S1 and are according to the ASTM standards.

2.2. Catalyst Synthesis

2.2.1. Mechanical Pre-Treatment of Rice Husk

In the pre-treatment process, at first, the collected rice husk (RH) was thoroughly rinsed with distilled water to remove contaminants and placed in an oven at $110\text{ }^\circ\text{C}$ for 24 h to eliminate any residual moisture content (MC) [41]. The dried RH was ground to a particle size of 0.5–1 mm using a microfine grinder (MF 10 BASIC, IKA, Staufen, Germany) with a speed range of 300–650 rpm and a frequency of 50–60 Hz, then sieved through a fine mesh sieve to obtain a uniform particle size, as shown in Figure 1.

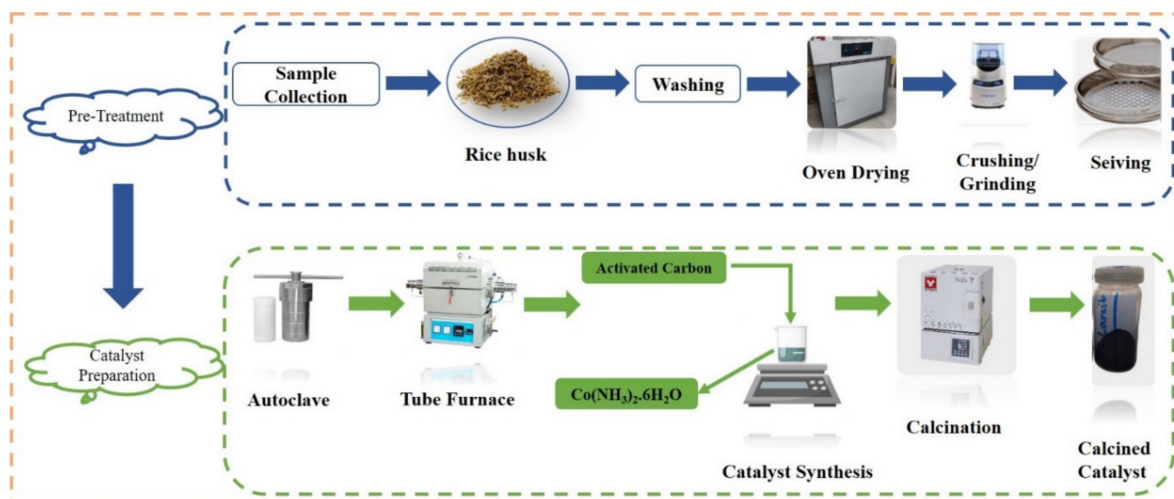


Figure 1. Schematic representation of co-loaded rice husk activated carbon.

2.2.2. Hydrochar Production by Hydrothermal Carbonization

Crushed 10 g of rice husk (RH) was added to 80 mL of deionized water and agitated at 750 rpm using a magnetic stirrer to achieve a homogenized mixture. The mixture was poured into a hydrothermal autoclave and then it was oven dried at $200\text{ }^\circ\text{C}$ for 7 h. After the reaction, the autoclave was cooled to room temperature, and the resulting hydrochar (HC) was collected. The calculated mass yield of the prepared hydrochar (HC) was 60.5%. The HC was rinsed with deionized water, filtered by grade 41 of Whatman filter paper (Maidstone, UK), and dried in the oven at $105\text{ }^\circ\text{C}$ for 24 h [30]. The resulting pH of the HC was 6.1 which is according to the literature range (5.0–7.5) [42], as shown in Figure 1.

2.2.3. Chemical Activation

The dried hydrochar (HC) was chemically activated using 2 g of HC impregnated with 1 M KOH solution and dried before processing in a tube furnace. Around 180 mL/min of nitrogen was pumped, and the tube was heated at $700\text{ }^\circ\text{C}$, with a ramp time of $5\text{ }^\circ\text{C}/\text{min}$ in the furnace. The furnace was allowed to cool once the set point had been maintained for 2 h before the nitrogen feed was turned off. The pH of the activated carbon was neutralized using deionized water, followed by a wash with a 0.5 M HCL solution and oven-dried

at 110 °C for 12 h. Ultimately, the obtained product is rice husk-based activated carbon (RHAC), as shown in Figure 1.

2.2.4. Preparation of Metal-Loaded Activated Carbon

The wet impregnation technique was employed to achieve metal loading on RHAC. A 0.05 molar of an aqueous solution of $\text{Co}(\text{NH}_3)_2 \cdot 6\text{H}_2\text{O}$ prepared, 5 wt.% of metal was loaded on the activated carbon. Then, the resulting slurry was placed in a beaker with a stirrer and heated at 80 °C until all the liquid evaporated. The leftover powdered solution was oven-dried at 110 °C for 24 h and calcined in the muffle furnace for 2 h at 300 °C (to eliminate nitrates). Regarding the metal load, the prepared sample was labeled RHAC-Co, as shown in Figure 1.

2.3. Catalyst Characterization

Fourier Transform Infrared Spectroscopy (Cary 630 FTIR, Agilent Technologies, Santa Clara, CA, USA) reveals sample structural changes. Ge-ATR multireflection with ATR diamond crystal is used. All samples' structural changes were analyzed with Microlab expert software (Cary 630) connected to the machine.

The use of X-ray diffractometry (XRD) allows for the examination of various characteristics of a sample, such as its level of crystallinity, its purity, and its unit cell dimensions. This analysis was performed using Bruker's D8 Advance X-ray diffractometer (Billerica, MA, USA) which features a $\text{Cu K}\alpha$ radiation source at a wavelength of 1.5 Å and was connected to a computer interface for data analysis.

A Scanning Electron Microscopy (SEM) and Energy dispersive spectroscopy (EDS) study of RHAC-Co was performed using JSM-6490LA Analytical Low Vacuum SEM (SEMTech solutions, Billerica, MA, USA).

Thermogravimetric analysis (TGA) was conducted to examine the thermal behavior of the catalyst samples using a SHIMADZU-DTG 60H instrument (Kyoto, Japan). The samples were subjected to temperature changes in a continuous nitrogen flow atmosphere (15 mL/min) from 20 °C to 800 °C.

Brunauer-Emmett-Teller (BET) analysis measures surface area whilst BJH identifies pore diameter and volume. At 77.25 K, the micromeritics ASAP 2010 device measured surface area and pore volume.

2.4. Biodiesel Production through Transesterification

Prior to transesterification, esterification was used to lower the high percentage of free fatty acid (FFA) in WCO, which could promote unintended saponification during transesterification [43]. The analysis of the waste cooking oil (WCO) revealed a high concentration of free fatty acids (FFAs). To produce biodiesel, the FFAs must be less than 3% which is 2.8%, as shown in Table S1. Thus, a two-step transesterification reaction was selected as the solution.

2.4.1. Esterification

Esterification of WCO with 3 wt.% Conc. H_2SO_4 as a catalyst decreased the acid value of the feedstock. The reaction was carried out at 55 °C for 3 h with an oil-to-methanol ratio of 1:6 [43]. The acid value was monitored by sampling at regular intervals until it dropped to <1, as shown in Table S1. After the mixture had settled, the oil layer was separated and heated to eliminate any extra methanol. The oil was then rinsed three times with water and dried in an oven for two hours at 100 °C to eliminate any remaining moisture and any unreacted alcohol. After that, the synthesized catalyst RHAC-Co was applied to perform the transesterification of waste cooking oil (WCO) with a low acid value as shown in Figure 2a.

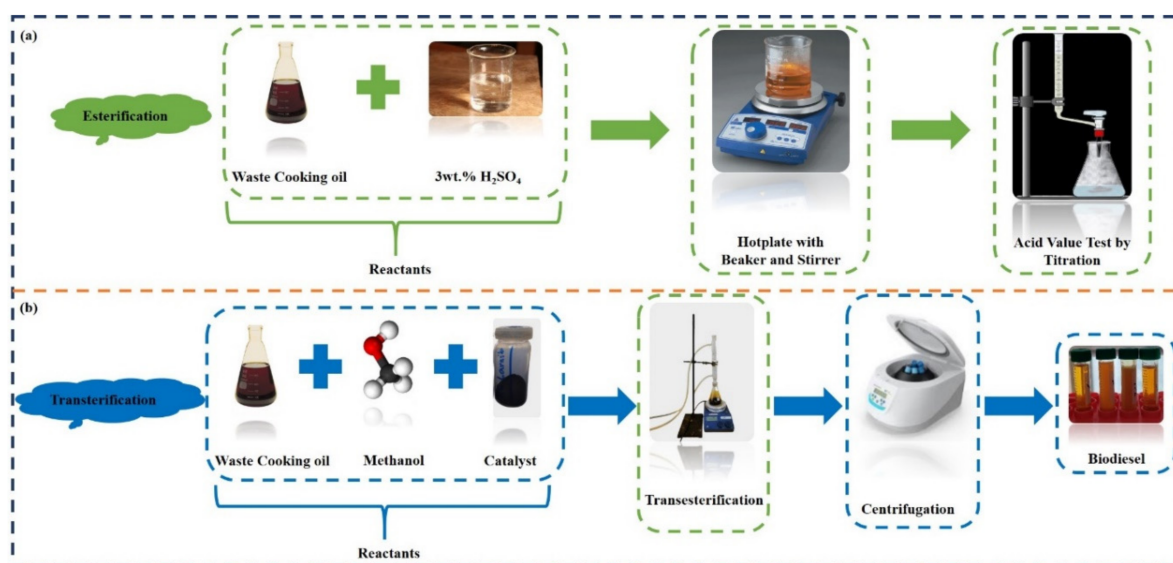


Figure 2. Experiment setup's figurative representation of producing biodiesel in two steps via (a) esterification and (b) transesterification.

2.4.2. Transesterification

Biodiesel production from WCO along with methanol and the loaded heterogeneous catalyst (RHAC-Co) was carried out on a laboratory scale through a series of optimization experiments. A 250 mL capacity flask was used to conduct the transesterification reaction. The flask was set up on a heating plate fitted with a magnetic stirrer and a temperature probe for precise control. Before adding methanol and catalyst to the reaction flask, WCO was preheated at 60 °C. The flask contained varying methanol-to-oil molar ratios ranging from 1:6 to 1:12, as part of the optimization process. The mixture of methanol-to-oil was agitated for 10 min with a catalyst concentration of 1 to 3 wt.% of RHAC-Co catalyst relative to the mass of WCO. After adding 25 mL of pre-heated WCO, the temperature of the mixture was varied from 60 to 90 °C, at intervals of 5 °C. The transesterification proceeded for a time duration ranging from 45 to 60 min under 750 rpm (for all experiments) of continuous stirring. To prevent methanol evaporation during transesterification, a condensing tube was fitted to the conical flask, as shown in Figure 2b. On completion of the reactions, the catalyst and the glycerol layer were separated from the solution by centrifugation and methanol evaporation [44]. For comparison, commercial KOH was used as a standard base catalyst combined with methanol before the esterified oil was added. Synthesized biodiesel was examined for quality and yield. Table 1 lists the independent variable ranges for transesterification.

Table 1. Lists the independent variable ranges.

Independent Variables	Value	(Lower–Upper)
Temp. (°C)	A	60–90
(M:O)	B	6–12
Catalyst Conc. (%)	C	1–3
Time (mins)	D	45–60

2.5. Characterization of Biodiesel

The flash point, specific gravity, calorific value, saponification value, viscosity, iodine value, cetane number, and yield were performed after transesterification. The biodiesel was tested as per ASTM standards (ASTM D6751) specifications [45].

Fourier Transform Infrared Spectroscopy (FTIR) (Cary 630 FTIR, Agilent Technologies, USA) was employed for the identification of functional groups present inside biodiesel. Ge-

ATR multireflection with ATR diamond crystal was used. All samples' structural change was analyzed with Microlab expert software connected to the machine.

The composition of Fatty Acid Methyl Esters (FAME) in the biodiesel sample is determined using the Shimadzu GCMS-QP2020 NX gas chromatograph-mass spectrometer. To accomplish this, 25 mg of the biodiesel sample is dissolved in 0.5 mL of n-hexane, resulting in a sample solution that is injected into the GC/MS for analysis and identification of the Fatty Acid Methyl Ester composition. The injection volume is set at 1 μ L with a split ratio of 20:1, and the initial set temperature is 150 $^{\circ}$ C with an initial retention time of 5 min. The maximum temperature is 220 $^{\circ}$ C with a ramp of 10 $^{\circ}$ C/min, and a maximum retention time of 5 min. The inlet temperature and detector transfer line temperature are set at 250 $^{\circ}$ C and 300 $^{\circ}$ C, respectively, while the electron impact ion source mode is set to 70 eV. The scan range is set at 30–500 m/z , and the ion source temperature and interface temperature are set at 200 $^{\circ}$ C and 250 $^{\circ}$ C, respectively.

2.6. Optimization Studies for Biodiesel Yield by Response Surface Methodology (RSM)

The response surface approach was investigated for its potential to optimize and predict biodiesel yield. In the Design Expert-13 software, a Central Composite Design (CCD) model was employed to study the independent variable effects on the prediction of the maximum biodiesel yield. This was done to make the most accurate prediction possible.

Experimental Design

Design Expert-13 devised the experimental layout, and a testable mathematical model was created using Central Composite Design (CCD). Temperature (T), the methanol-to-oil molar ratio (M:O), the catalyst concentration (wt.%), and reaction time (t) were outlined as the four independent factors for transesterification. Table 1 lists these independent variables' ranges. Experiments were run with an M:O molar ratio between 1:6 and 1:12, with a temperature range of 60–90 $^{\circ}$ C, reaction time between 45 and 60 min, and a catalyst concentration of between 1 and 3 wt.%. Within the context of Equation (1), the term "system reaction" in response surface methodology (RSM) refers to the relative fraction of biodiesel volume to feed volume [46].

$$\text{Biodiesel yield} = \frac{\text{Volume of Biodiesel}}{\text{Volume of Feed}} \times 100 \quad (1)$$

The greater ranges and depths of the independent factors lend greater credibility to the CCD-based RSM approach. The RSM approach allows for the assessment of both the independent variable's effect and the interaction between factors. In addition, you may identify which parameters, or parameter combinations, significantly alter the system's reaction. Based on Equation (2), we can get the required number of experiments (N) for a system with a factor (f), which is a number of independent variables [47].

$$N = 2^f + 2f + C_0 \quad (2)$$

where C_0 equals the number of central points. The response surface approach produces quadratic equation models.

3. Results and Discussion

3.1. Catalyst Characterizations

3.1.1. Fourier Transform Infrared Spectroscopy (FTIR)

FTIR is an analytical technique for the study of structural changes in chemical compositions, the determination of structural similarity between pure materials, and the investigation of structural changes in biomass as a result of thermal or chemical processing, as shown in Figure 3.

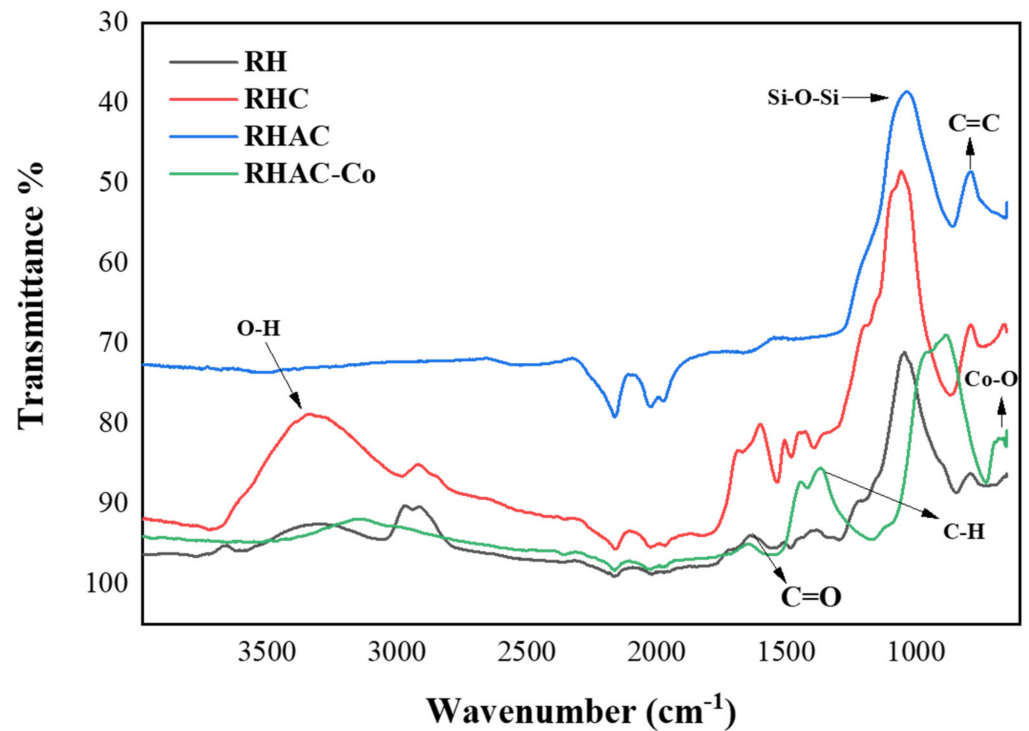


Figure 3. Fourier Transform Infrared Spectroscopy (FTIR) peaks of catalyst at various stages RH, RHC, RHAC, and RHAC-Co.

In this study, FTIR analysis was carried out to identify the functional groups of four samples including RH, RHC, RHAC, and RHAC-Co, and to identify any changes in structural analysis after treatments such as HTC, chemical activation, and wet impregnation. The study found a peak at 3200–3250 cm^{-1} , indicating an O-H stretch of alcohol was present in the samples due to the presence of moisture [41]. As thermal treatments were applied, this peak almost diminished. The Si-O-Si antisym stretch at 1100–1000 cm^{-1} was the most significant peak for all four samples since silica is the most crucial component in the rice material's chemical structure. However, it continued to be present with different temperature stages [30]. Another peak at 780 cm^{-1} shows the C=C bending and the peak at 1380 cm^{-1} indicates the presence of methylene group C-H in the developed catalyst (RHAC-Co) as a new entity after loading [48]. The Co-O peaks near 660 cm^{-1} implied that the RHAC-Co catalyst contained cobalt [49], agreeing with the XRD results. This finding was also reported by Li et al. [48], who used cobalt-loaded cherry biochar as a heterogeneous catalyst.

3.1.2. X-ray Diffraction (XRD)

Figure 4 represents the XRD profile of RHAC and RHAC-Co. The diffraction pattern of RHAC activated at 750 °C using KOH displayed broad diffraction peaks with no distinct peaks, indicating a primarily amorphous structure [50]. The RHAC sample featured two broad peaks around $2\theta = 26^\circ$ and 43° , which can be attributed to reflection from the (100) and (002) planes [50,51]. This is characteristic of amorphous carbon with disordered carbon rings, indicating a small degree of microcrystallinity and a turbostratic graphite structure [52]. This supports preliminary studies by Nazzal et al. [53], which have reported that the broad peaks observed in AC samples are indicative of graphite-like microcrystallites bound by a cross-linking network consisting of multiple graphite-like layers. The diffraction spectra of the RHAC-Co catalyst displayed discrete peaks of cobalt oxide crystallites at 26.5° , 31.5° , 36.82° , 59.5° , and 65.7° , similar to the previously reported study [54]. Furthermore, the absence of peaks from potential contaminants like nitrates in the RHAC and RHAC-Co

samples, confirms the effectiveness of the washing process in achieving purity for the activated carbon and loaded catalyst [55].

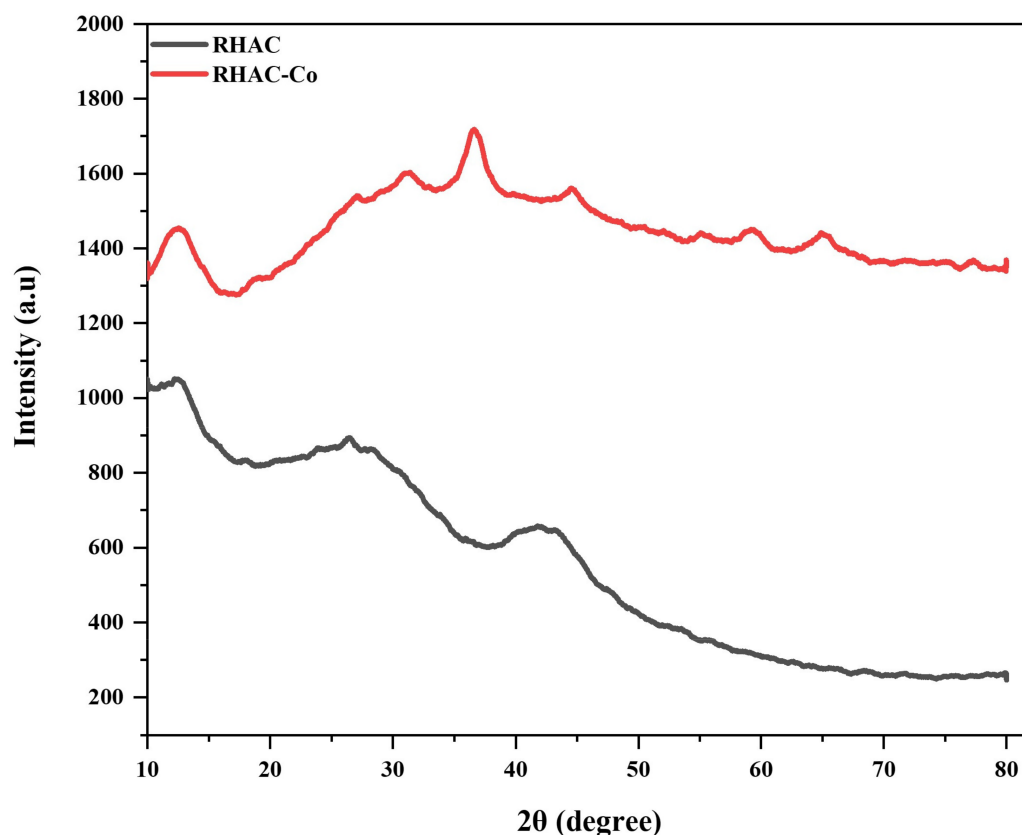


Figure 4. X-ray diffraction (XRD) analysis of RHAC and RHAC-Co.

3.1.3. Scanning Electron Microscopy (SEM) and Energy Dispersive X-ray Spectroscopy (EDS)

SEM images of the RHAC and RHAC-Co are shown in Figure 5a,b. The external surfaces of these RHACs reveal irregular large cavities, suggesting that the porosity of the material was created due to adding KOH reagent at 700 °C for activation. Pore development in the RHAC resulted in enhanced pore volume and surface area of the RHAC by promoting the dispersion of KOH molecules into the pores [50]. This microporosity could further help in the adsorbing characteristics of this material [56]. After loading with the cobalt catalyst, the pores of RHAC were completely covered with the cobalt particles, as shown in Figure 5a. Figure 5b shows the presence of specks of cobalt oxides, which depicted a brighter zone within the larger particles. The same bright specks were shown in the literature [54]. It was found that the cobalt oxide particles were well assimilated in the carbon samples. The Co-AC catalyst sample consisted of a partially agglomerated mixture of irregularly shaped small and large particles in terms of morphology and cobalt distribution (non-uniform distributions) [57]. The elemental composition of RHAC-Co was verified by energy dispersive spectroscopy analysis (EDS) (in Supplementary Data) with a detector mounted on a microscope, as shown in Figure S1. The composition of RHAC-Co is made up of 56.5% carbon, 27.4% oxygen, 11.3% silicon, 2.3% cobalt, 0.1% potassium, 1.9% iron, and 0.5% calcium, as shown in Figure S1. By incorporating metal oxides, the catalyst is endowed with basic surface sites and a large surface area, greatly enhancing its performance in the transesterification reaction [58]. The potassium in the catalyst contributes to its high basicity and is responsible for its exceptional catalytic activity. Similar results have been observed in other heterogeneous solid base catalysts made from different biomass sources such as banana peel [7], tucumã peels [59], walnut shell [60], and *Sesamum indicum* [61].

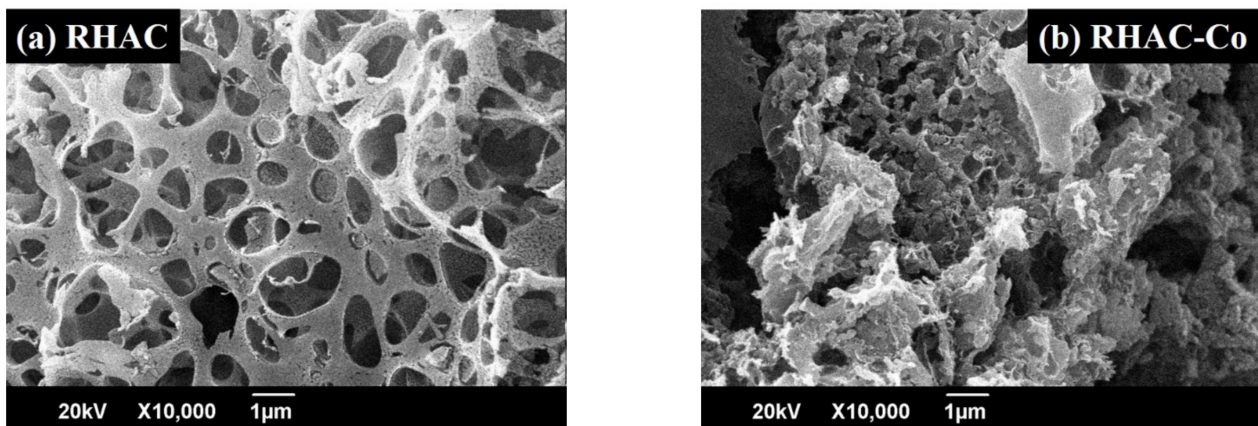


Figure 5. Scanning Electron Microscopy (SEM) graphs.

3.1.4. Thermo-Gravimetric Analysis (TGA)

Figure 6 shows the TGA analysis of the prepared RHAC before its loading with the metal, to study thermal stability. The thermal stability of the RHAC was compared with the RHC. It is clear from both samples that there is a minor loss before 80 °C; this is due to the elimination of moisture. The presence of moisture in the samples may have been absorbed from the environment during handling and storage. For up to approximately 300 °C, the samples remained relatively constant with only slight degradation. According to scientific consensus, this slight decomposition phase was likely a result of the breakdown of low molecular weight products. However, in RHC, an observable loss between 310 and 550 °C appeared. That happened because the degradation of celluloses and hemicelluloses present inside the precursor (75% mass loss) releases volatile matter [53,62]. At elevated temperatures, up to 600 °C, the sample mass experienced a reduction, retaining only 18% of its initial mass, indicating the breakdown of lignin which is a stable structural component [50]. Additionally, the thermogram of RHAC showed a final average yield of 69% even after being heated up to 800 °C, indicating high thermal resistance.

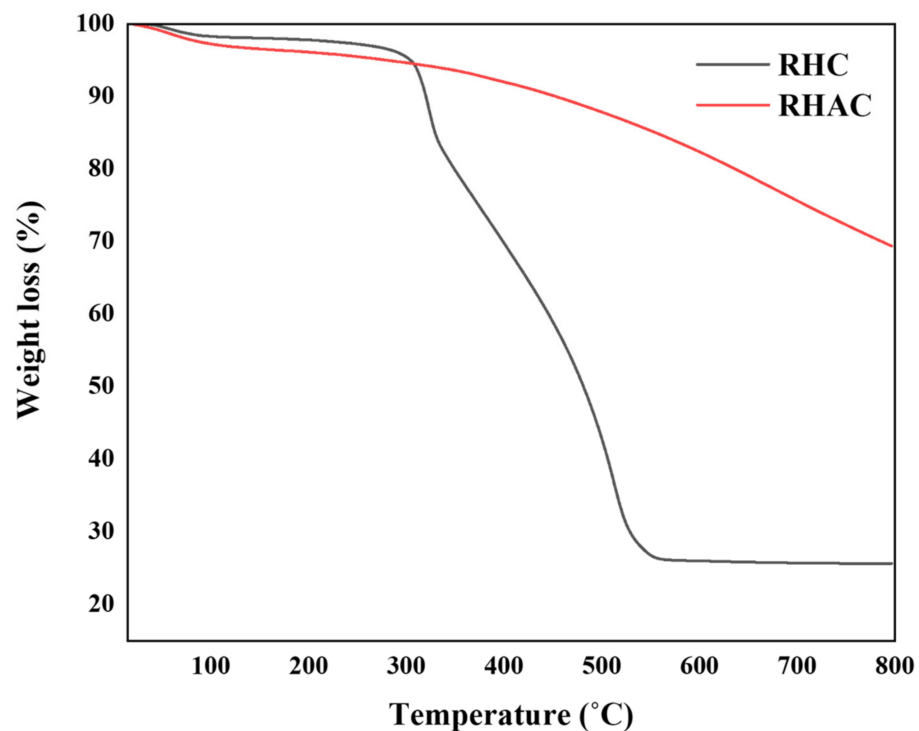


Figure 6. Thermogravimetric analysis of RHC and RHAC.

3.1.5. BET Analysis

An elevated BET surface area of $1219 \text{ m}^2 \text{ g}^{-1}$ was observed by the RHAC used along with a microporous structure, having a significant porous volume of $0.49 \text{ m}^3/\text{cm}^3$. However, the introduction of metal particles to the RHAC was anticipated to result in a decrease in the surface area [36]. Guo et al. [63] have demonstrated that lower surface areas in catalysts often indicate an increased concentration of basic sites present inside solid catalysts' interiors. This characteristic can aid in the transesterification process by facilitating the diffusion of glyceride into the interior of the catalyst [11], as shown in Table 2.

Table 2. BET analysis of RHAC and RHAC-Co.

Type	Surface Area (m^2/g)	Pore Size (\AA)
RHAC	$1219.618 \text{ m}^2/\text{g}$	14.9
RHAC-Co	$324.984 \text{ m}^2/\text{g}$	11.3

3.2. Biodiesel Yield Characterization

3.2.1. Esterification

The optimal conditions for reducing the FFA content in WCO were determined to be a mixture of 60 mL of methanol and 3% sulfuric acid, agitated at $55 \text{ }^\circ\text{C}$ for 3 h at 300 rpm. This process successfully reduced the acid value from $7 \pm 0.02 \text{ mg}$ of KOH/g of oil to $3 \pm 0.01 \text{ mg}$ of KOH/g of oil.

3.2.2. Physio-Chemical Properties of Produced Biodiesel through Transesterification

The flashpoint of RHAC/Co-BD was recorded at $140 \text{ }^\circ\text{C}$, which is higher compared to conventional diesel and meets the standard requirement of $130 \text{ }^\circ\text{C}$ or above for biodiesel. This makes RHAC/Co-BD a safer alternative to conventional diesel [64]. The standard reference sample, KOH-BD, had a flashpoint of $130 \text{ }^\circ\text{C}$. Biodiesel's specific gravity ranges from 0.86 to 0.90, with the standard reference sample KOH-BD having 0.9, and RHAC/Co-BD 0.88. The specific gravity of biodiesel is influenced by the composition of fatty acids and the presence of both free and bound glycerin. Biodiesel with a higher density provides greater energy and improves the mileage and power of engines. This is because denser vegetable oils tend to produce denser biodiesel since the specific gravity is determined by the concentration of fatty acids [65]. The viscosity of biodiesel plays a role in both the combustion quality of the fuel-air mixture and the formation of biodiesel droplets. Both extremely low and high viscosity levels can negatively impact engine performance. When combustion is inefficient, black smoke may be produced as a result of poor viscosity and lack of penetration. Additionally, if the fuel is too viscous, it may have difficulty flowing through the injector and could potentially freeze the cylinder wall, reducing the amount of fuel that is burned [66]. For KOH-BD and RHAC/Co-BD, the WCO biodiesel was found to have a viscosity of 3.74 and $5.72 \text{ mm}^2/\text{s}$, respectively. This is a normal value, falling between the ranges of 1.9 and $6.0 \text{ mm}^2/\text{s}$ (ASTM D6751-02, 2002) [67]. To ensure the accuracy of the pH measurement, three calibration tests were conducted prior to analysis. The measured pH value was approximately 7.5, which aligns with recommendations in the literature for optimal biodiesel production. Maintaining a pH of around 7.5 is important as it helps minimize the risk of corrosion to engine parts, enhances oxidative stability, and supports the shelf life and performance of biodiesel in engines [68], while in literature for KOH-BD, it is reported in the range of 8–10 [69]. The calorific value, or energy content, of biofuels, is a significant characteristic for comparing their properties to that of conventional diesel fuel [70]. Lower energy contents can impact key performance parameters, such as maximum horsepower and torque [71]. Industry standards generally consider biodiesel to have a calorific value of around $37.27 \text{ MJ}/\text{kg}$. The energy density and calorific value of biodiesel can vary, based on the type of feedstock used and the method of production

applied. The calorific value of the RHAC/Co-BD was 40.07 MJ/kg, while the standard reference sample KOH-BD had a calorific value of 46.05 MJ/kg.

Engine performance is substantially impacted by the density of biodiesel. To ensure efficient combustion in the engine, the density of the biodiesel must be within a specific range to achieve the optimal air-fuel mixture. High-density diesel is unacceptable because it can result in incomplete combustion and the release of particulates, however, this issue can be resolved by blending conventional diesel with biodiesel. Diesel has a standard density of 848 kg/m³, while biodiesel ranges from 870 to 900 kg/m³ [64]. Higher than conventional diesel fuel, biodiesel has a density of about 0.88 g/cm³ (870 kg/m³–900 kg/m³). Calculated density for WCO biodiesel showed that RHAC/Co-BD had a density of 899 kg/cm³, which is consistent with the fuel standard (ASTM standard). A saponification value higher than 312 mg KOH g⁻¹ of oil leads to soap formation and decreases the yield and quality of biodiesel. The synthesized biodiesel shows lower saponification values than the ASTM 6751 standard, where the RHAC/Co-BD depicts the lowest value of 193.4 mg KOH g⁻¹. Biodiesel's degree of unsaturation can be quantified by measuring its iodine number; this provides valuable insight into the oil's stability. Fuel polymerization occurs when unsaturation levels are high because epoxides are formed when oxygen is added to double bonds [72]. Biodiesel should have an iodine number of 120 g I₂/100 g oil. The iodine content of KOH-BD, in the standard sample, was 57.5 g I₂/100 g, while that of RHAC/Co-BD was 61.32 g I₂/100 g. The cetane number of biodiesel is determined by the carbon number of the fuel and the concentration of Fatty Acid Methyl Ester (FAME). The ideal range for biodiesel is between 46 and 52, while for conventional diesel, it's 40 and 55. The reference sample KOH-BD had a cetane number of 50.5, while RHAC/Co-BD had 51. The synthesized biodiesel is better since the samples have the right FAME and carbon numbers. The choice of substrate, catalyst, and other reaction factors greatly affect how much biodiesel is produced with the amount of substrate utilized [66]. Because of this, the outcomes of product yield alter when these reactants and reaction circumstances change. The product yield after performing transesterification reactions using synthesized catalysts was 96.3% for (RHAC/Co-BD), and 98.33% for (KOH-BD) standard catalysts, as shown in Table 3. Further optimization-based analysis using RSM was conducted on the RHAC/Co-BD sample to determine the impact of various independent variables on the final yield.

Table 3. Comparison of physicochemical characteristics between RHAC/Co-BD and standard KOH-BD.

Properties	Unit	BD Standards (ASTM 6751) [73]	KOH-BD	RHAC/CO-BD
Flashpoint	°C	>130	130	140
Specific gravity	----	0.86–0.90	0.9	0.88
Viscosity	mm ² /s	1.9–6.0	3.74	5.72
Density	kg/m ³	870–900	900	899
pH	----	6.5–7.5	8–10	7.5
Calorific Value	MJ/Kg	>35	46.048	40.068
Saponification Value	mg KOH/g	<312	112.2	252.45
Iodine Value	g I ₂ /100 g oil	<120	57.5	60
Cetane Number	----	≥ 47	50.5	51
Yield	(%)	94	98.33	96.3

3.2.3. Fourier Transform Infrared Spectroscopy (FTIR)

The alkane C-H bonds' existence is observed in the wave number's range of 2800–3000 cm⁻¹ and 1400–1500 cm⁻¹ on the biodiesel's FTIR spectra. Figure 7 also indicates the presence of an oxygen functional group namely the ester C–O bond in the 1000–1300 cm⁻¹ range. Furthermore, the ester C=O bond in 1735–1750 cm⁻¹ was also observed. Contrary to conventional diesel, the present biodiesel is much cleaner and leads to complete combustion due to the presence of oxygen. These FTIR results match the findings from prior studies

in the literature [44,74]. The biodiesel produced from different catalysts, such as KOH-BD and RHAC/Co-BD, showed the same functional group peaks of C-H and C-O bonds as shown in respective Figure 7.

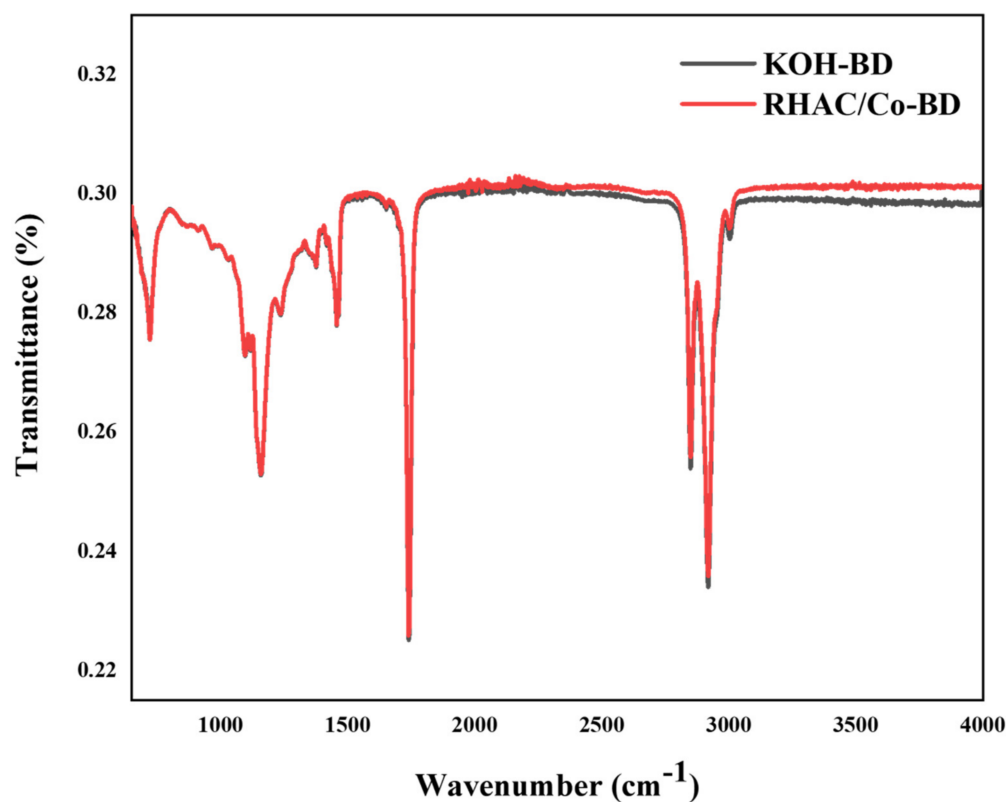


Figure 7. Fourier Transform Infrared Spectroscopy of RHAC/Co-BD and conventional KOH-BD.

3.2.4. Gas Chromatography-Mass Spectroscopy (GC-MS)

Figure 8 and Table 4 display the retention period and fragmentation pattern data from GC analysis, which reveals six primary distinctive FAME peaks. FAME composition and common names in biodiesel under optimal conditions are determined. However, the GC analysis shows that the highest possible biodiesel mass yield was 96.3%. The percentage of FAME present was roughly 93.89% by weight, while the efficiency of conversion reached 90.38%.

Table 4. Fatty Acid Methyl Ester (FAME) content present in RHAC/Co-BD.

Peak(s)	Fatty Acid Methyl Ester (s) (FAME)	Common Name	Formula	Retention Time (min)	Composition (%)
1	Hexadecanoic acid methyl ester	Methyl palmitate	C ₁₈ H ₃₆ O ₂	22.942	28.56
2	Octadecanoic acid methyl ester	Methyl Stearate	C ₁₈ H ₃₆ O ₂	25.305	21.98
3	<i>cis</i> -9-Octadecenoic acid methyl ester	Methyl Oleate	C ₁₈ H ₃₄ O ₂	24.540	15.30
4	<i>cis</i> -9- <i>cis</i> -12-Octadecadienoic acid methyl ester	Methyl linoleate	C ₁₈ H ₃₂ O ₂	23.575	15.67
5	<i>cis</i> -9,12,15-octadecatrienoic acid	Methyl Linolenate	C ₁₈ H ₃₀ O	26.432	6.50
6	Pentadecanoic acid, 14-methyl-, methyl ester	Methyl pentanoate	C ₁₇ H ₃₄ O ₂	21.167	5.88
					Total = 93.89%

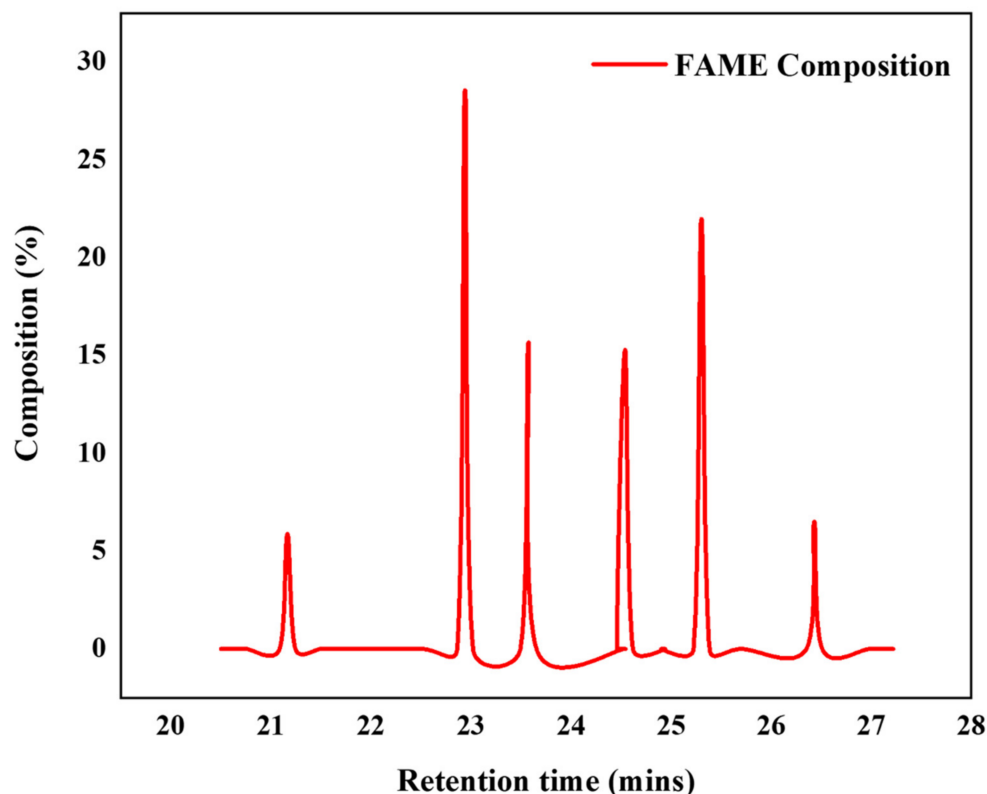


Figure 8. Fatty Acid Methyl Ester (FAME) peaks.

3.3. Optimization Studies for Biodiesel Yield by RSM

As shown in Table 5, 30 experiments using the CCD method were conducted and their respective biodiesel yields were recorded. According to the findings, the highest yield of biodiesel was achieved in the 3rd run at 96.3%. To ensure the accuracy of the results, various figures were analyzed, including a graph comparing predicted and actual values, as shown in Figure S2. A close correlation between observed data and RSM predictions is indicated by the clustering of points close to the line $y = x$. To validate the results of the RSM, an Analysis of Variance (ANOVA) was conducted. Table 6 of the ANOVA findings shows that model terms A, C, D, AB, AC, CD, A^2 , B^2 , C^2 , and D^2 are significant (their p -values are less than 0.0500), while model terms with p -values more than 0.1000 are not significant. R^2 and R^2 adj, which highlight the importance of the Quadratic model, were also calculated to ascertain the model's precision. By comparing actual and predicted values, we find that the model provides a high level of accuracy for estimating process yield ($R^2 = 0.9723$). Table 7 displays the estimated RSM optimum values for the factors, with a maximum output of 96.3%. To validate the RSM's predictions under practical conditions, independent trials under ideal conditions were conducted twice. Both trials confirmed the model's prediction, with an average biodiesel yield of 96.3% observed in each case. The obtained experimental value for yield is in accordance with the predicted experimental value. Further, the yield value is in accordance with the predicted values given by the RSM model in the literature [7]. These results not only affirm the reliability of the RSM model but also suggest that the optimal settings identified can be confidently applied in practice with minimal error.

Table 5. CCD matrix with four independent variables and experimental response.

Runs	Factor 1, A: Temperature (°C)	Factor 2, B: M:O (mol/mol)	Factor 3, C: Catalyst Concentration (wt.%)	Factor 4, D: Time (min)	Response 1 Yield (%)
1	90	6	1	60	87.9
2	75	15	2	52.5	94
3	75	9	2	52.5	96.3
4	60	12	3	45	88
5	90	6	3	45	92
6	75	9	2	52.5	96.5
7	60	12	1	45	89
8	75	9	2	67.5	88.5
9	60	6	1	45	88.2
10	60	12	1	60	91.25
11	75	9	4	52.5	86.5
12	90	12	3	60	93.5
13	60	6	1	60	86.45
14	90	12	1	45	88.5
15	75	3	2	52.5	92.45
16	90	6	1	45	89.5
17	75	9	2	52.5	96.3
18	105	9	2	52.5	90.5
19	90	6	3	60	92.45
20	60	12	3	60	89.5
21	75	9	0	52.5	83
22	75	9	2	52.5	96.3
23	45	9	2	52.5	88.15
24	75	9	2	52.5	96.3
25	90	12	1	60	87.5
26	60	6	3	45	87
27	60	6	3	60	89.45
28	90	12	3	45	90
29	75	9	2	52.5	96.3
30	75	9	2	37.5	85

Table 6. ANOVA for biodiesel yield.

Source	Sum of Squares	df	Mean Square	F-Value	p-Value	
Model	413.31	14	29.52	37.65	<0.0001	significant
A-Temp.	12.33	1	12.33	15.72	0.0012	
B-M:O	2.28	1	2.28	2.91	0.1087	
C-Catalyst Conc.	17.68	1	17.68	22.55	0.0003	
D-Time	6.83	1	6.83	8.71	0.0099	
AB	5.06	1	5.06	6.46	0.0226	
AC	15.02	1	15.02	19.15	0.0005	
AD	0.6006	1	0.6006	0.766	0.3953	
BC	1.05	1	1.05	1.34	0.2652	
BD	2.81	1	2.81	3.58	0.078	
CD	6.25	1	6.25	7.97	0.0128	
A ²	74.49	1	74.49	94.99	<0.0001	
B ²	12.42	1	12.42	15.84	0.0012	
C ²	213.76	1	213.76	272.62	<0.0001	
D ²	144.05	1	144.05	183.71	<0.0001	
Residual	11.76	15	0.7841			
Lack of Fit	11.76	10	1.18			
Pure Error	0	5	0			
Cor Total	425.07	29				
	R ² = 0.9723	-		R ² _{adj} = 0.9465		

Table 7. Optimum result yielded by Resource Surface Methodology.

Item	Temp. °C	M:O mol/mol	Catalyst Conc. wt.%	Time min	Yield %
Value	75	9	2	52.5	96.3

Interaction Effect of Independent Variables for Yield Studies

To evaluate the effect of independent variables on biodiesel production, three-dimensional figures are utilized, and two factors are compared at a time, while the other two factors are kept at optimal levels. Response Surface Methodology (RSM) analysis is used to study the impacts of the variables, and the graphs of the model exhibit quadratic behavior. This approach is employed to identify the optimal conditions for biodiesel production, given in Figure 9a–f.

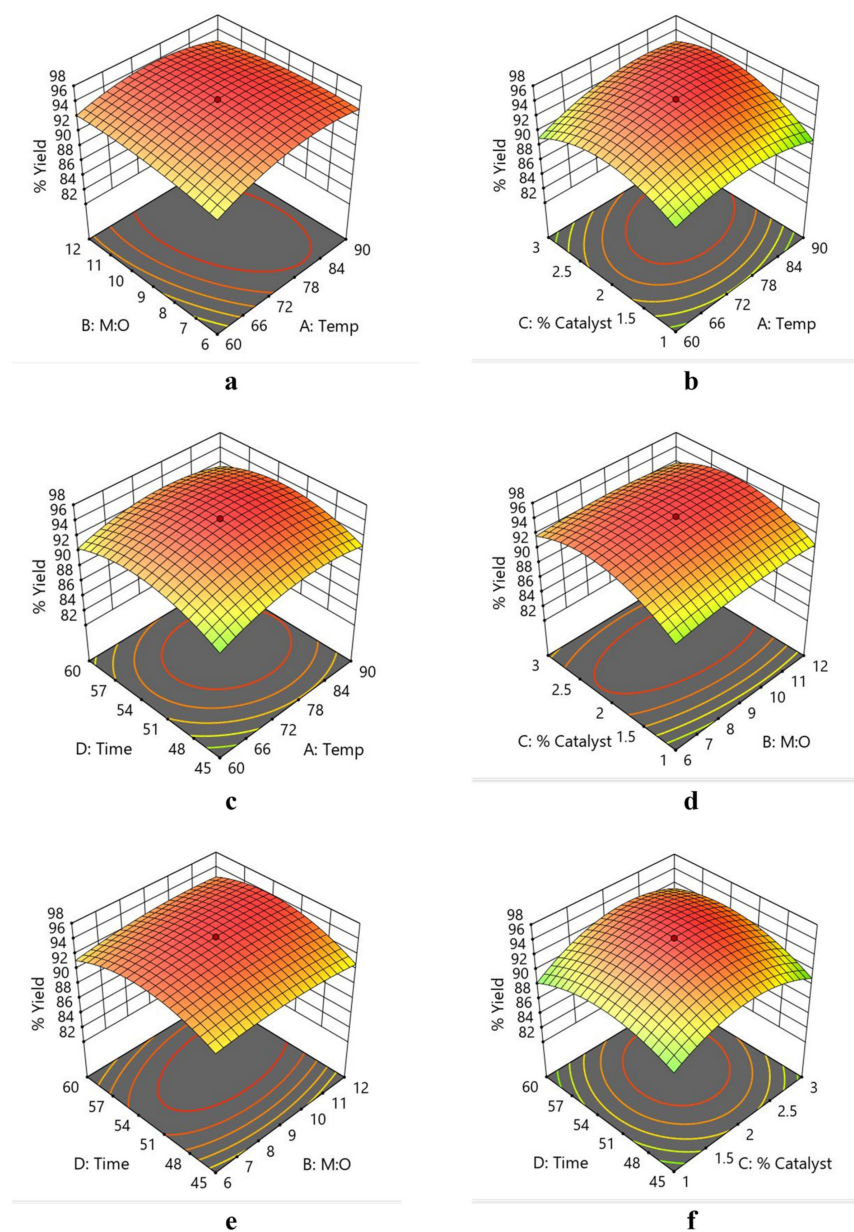


Figure 9. 3D response surface plots for comparison: (a) temperature vs. methanol to oil ratio, (b) temperature vs. catalyst, (c) temperature vs. time, (d) M:O vs. catalyst, (e) M:O vs. Time, and (f) catalyst vs. time.

Figure 9a demonstrates yield response to temperature and M:O variables at the optimal time and catalyst concentration. As could be observed, the biodiesel yield was slightly lower at 60 °C, compared to 75 °C, and when this temperature was held at 60 °C and 75 °C the biodiesel yield increased with an increase in the M:O ratio, but as the M:O ratio reached about 12:1 there was a sharp drop in the yield at both temperatures. The reason could be that the higher quantity of methanol might have increased the glycerin solubility in the reaction mixture causing a reverse glycerolysis reaction to occur [75].

Figure 9b demonstrates yield response to temperature and catalyst conc. variables at the optimum time and M:O ratio. With an increment in temperature from 60 °C to 75 °C, the yield increased with an increase in the catalyst conc., but at catalyst concentration more than 2 wt% roughly, the yield dropped dramatically due to soap formation and lower conversion from triglyceride to FAME [76]. By comparing Figures 9a and 9b, it is clear that when temperatures are above 60 °C, the impact on the yield is similar for the catalyst concentration and the M:O ratio.

Figure 9c demonstrates yield response to temperature and time variables at optimum catalyst conc. and M:O molar ratio. At 60 °C, the layer of biodiesel was not clear (viscous), also the density was higher from glycerol, so to tackle that, the temperature was raised to 75 °C which gave the highest yield of 96.3%. So, it's clear that up to 75 °C, the effect of temperature is more important than that of reaction time. However, the increase in temperature decreases the retention time from 60 to 52.4 min, while giving the highest yield. Likewise, a previous study found that high temperatures enhanced the reaction by reducing retention time. The phases separated at around 0.5 h at higher temperatures, compared to 0.25 h at lower temperatures [76].

Figure 9d demonstrates the yield response to M:O and catalyst conc. variables at optimum time and temperature. A higher concentration of catalyst (more than 1.8%) and a higher molar ratio of M:O (greater than 8.5) result in the highest yield. Here, the heterogeneous catalytic process required a somewhat larger M:O molar ratio. Excess methanol over the optimum ratio has been shown in several studies to reduce yield by reducing the amount of catalyst that comes into contact with the oil [77]. Developing the oil-alcohol interface requires increasing both the methanol concentration and the catalyst concentration. The reaction kinetics consequently improves with an increase in the interface [46].

The effect of M:O ratio vs. time on yield at optimum catalyst conc. and temperature is demonstrated in Figure 9e. This suggests that going from an M:O ratio of 8.5 to 9.0 boosts yield by a factor of 1.5 when the reaction time is increased from 45 to 52.5 min. It is possible to claim that when reaction time increases, the rate of conversion of FAME also increases. Owing to the initial mixing and dispersal of the alcohol into the oil, the reaction starts slowly. The reaction speeds up steadily and rapidly with time. At 50 min, the yield is at its highest and remains roughly stable with additional increases in reaction time. Based on this data, it appears that a response time of 48–53 min is optimal. However, if the reaction period exceeds 60 min, the product yield will decrease due to the reverse reaction of transesterification, which will cause esters to be lost and more fatty acids to form soaps. A higher molar ratio for a given time boosts methyl ester synthesis, as reported in a previous study. Considering the same rationale, the findings of that study yielded an equivalent of 94.9%, while in our instance it was 96.3% [78].

Figure 9f illustrates biodiesel yield response to time and catalyst concentration. At the optimal temperature, the catalyst's effect on yield was examined between 1 and 3 wt.% under 45–60 min reaction periods. Biodiesel yielded 96.3% at 2 wt.% catalyst. For a 3 wt.% catalyst, increasing concentration gradually decreased yield by 87%. This indicates soap production due to extra catalyst and slower triglyceride to FAME conversion, which reduced biodiesel yield. The most biodiesel was yielded at 52.4 min with 2 wt.% catalysts. A heterogeneous catalyst made from pyrolyzed rice straw and sulfonated was compared in an earlier literature search. Transesterification yielded 97% biodiesel in approximately 6 h [79]. In this study, the catalyst cuts time by 85%.

3.4. Significance of Using RHAC-Co Catalyst

The use of activated carbon support (RHAC) in this study is unique compared to other support materials, as shown below in Table 8, as it is derived from a renewable resource, namely rice husk, making it an environmentally friendly and sustainable option. Furthermore, this study is distinguished by the use of waste cooking oil (WCO) as a feedstock, which poses challenges due to its tendency to become rancid, but these issues were overcome during the esterification process. Despite this challenge, WCO offers benefits such as energy security, recyclability, and pollution reduction. Cobalt immobilization on activated carbon support (RHAC) shown in this study is a novel approach then other cobalt-containing composite materials towards transesterification. Our study has advantages over others in efficiency, eco-sustainability, facile separation, and green pathways toward innovative catalyst synthesis. The use of transition metal catalysts, like cobalt, is important due to their ability to form robust bonds with oxygen atoms in ester groups of oil, facilitating transesterification reactions. Cobalt's easy immobilization on activated carbon support (AC) makes it a convenient catalyst for biodiesel production, and its incorporation into RHAC enhances its catalytic performance due to the presence of active basic sites improving process efficiency. Furthermore, for heterogeneous catalysts, the ability to be reused is necessary. An intriguing fact is that the catalyst retained its action after being used three times. Productivity dipped after the fourth cycle, most likely because the active site leached to the surface.

Table 8. Relative catalytic performance using cobalt-modified catalysts for transesterification.

Catalyst	Oil Used	Synthesis Route	Operating Parameters				Conv.	Ref.
			Temp.	M:O	Catalyst Conc.	Time		
Co-CaO	Microalgal biomass	Catalyst Prep.: Co-precipitation impregnation route Transesterification	65 °C	3:1	0.2%	120 min	98%	[58]
Co-ZnO	Mesua ferrea oil	Esterification/Transesterification Transesterification	60 °C	9:1	2.5%	180 min	98.03%	[80]
Co/Femixed Oxides	Cooking oil	(Catalyst Layered Doubled Hydroxides)	65 °C	6:1	2%	20 min	96%	[81]
MgCoAlLa-LDH	Canola oil	Ethanol Transesterification Cat. Prep.: Co-precipitation	100 °C	16:1	1%	300 min	95%	[82]
CoO-NiO promoted sulphated ZrO ₂	Oleophilic oil	impregnation route Transesterification	65 °C	3:1	0.2%	120 min	98.80%	[83]
RHAC-Co	Waste cooking oil	Esterification/Transesterification Catalyst Prep.: Wet impregnation	75 °C	9:1	2%	52.5 min	96.3%	This work

4. Conclusions

In conclusion, a new solid transition metal loaded biomass-derived heterogeneous catalyst called RHAC-Co was prepared that showed great catalytic activity towards transesterification and was characterized using XRD, FTIR, SEM-EDS, TGA, and BET. Rice husk-derived activated carbon (RHAC) was used as a support material due to its sustainability, high surface area, porosity, and thermal stability. The addition of transition metal cobalt to RHAC resulted in a composite RHAC-Co with superior catalytic activity to RHAC. These properties make it an attractive support material for the loaded catalyst RHAC-Co. The green catalyst is justified by the analysis. The catalytic activity of the composite RHAC-Co was found to be superior to that of RHAC, likely due to the presence of active basic sites and cobalt metal. SEM-EDS analysis confirmed the presence of these elements Co, K, and Ca in the catalyst, which likely aided in the transesterification process. BET analysis also revealed that the addition of transition metal cobalt caused a reduction in the surface area from 1219 m²/g of RHAC to 324.984 m²/g of RHAC-Co and pore volume from 0.48 of RHAC to 0.16 m²/cm³ of RHAC-Co, suggesting that a decrease in surface area can lead to an increase in the concentration of basic sites within the catalyst and further promotes the transesterification process. The loaded catalyst was effectively used in the transesterification of waste cooking oil (WCO) and methanol, achieving a maximum biodiesel yield of 96.3%, in line with ASTM standards. The optimum conditions for this 96.3% yield were determined to be a temperature of 75 °C, an Oil/Methanol ratio of 1:9,

2 wt.% of RHAC-Co, and a reaction time of 52.5 min. Response surface methodology (RSM) was used to optimize the reaction parameters and showed that it is a good tool for yield optimization, by studying the interrelation between independent variables. Future research should focus on using this biodiesel for engine performance evaluation, environmental impact, and combustion characteristics along with the scaling up of the catalyst by optimizing it for commercial production.

Supplementary Materials: The following supporting information can be downloaded at: <https://www.mdpi.com/article/10.3390/su16177275/s1>, Figure S1: Elemental composition of RHAC-Co by energy dispersive spectroscopy analysis (EDS), Figure S2: Comparing the actual-predicted deviation; Table S1: Physiochemical properties of Waste cooking oil (WCO).

Author Contributions: Conceptualization, R.L., M.A. and M.K.; Methodology, L.A.K., M.A., M.K. and A.H.k.; Software, L.A.K., M.K., M.S. and A.B.; Data Curation, R.L., L.A.K., M.A. and M.K.; Validation, M.A., M.K. and W.U.H.K.; Visualization, R.L., M.A., M.K. and M.S.; Formal Analysis, M.S. and A.B.; Investigation, R.L., M.A. and M.K.; Writing—original draft, L.A.K., W.U.H.K.; Writing—review & editing, R.L., M.A. and M.K.; Supervision, R.L. and M.S.; Funding acquisition, M.S. and M.K. All authors have read and agreed to the published version of the manuscript.

Funding: This research work was funded by Institutional Fund Projects under grant no. (IFPIP: 454-829-1443). The authors gratefully acknowledge the technical and financial support provided by the Ministry of Education and King Abdulaziz University, DSR, Jeddah, Saudi Arabia.

Institutional Review Board Statement: Not applicable.

Informed Consent Statement: Not applicable.

Data Availability Statement: The original contributions presented in the study are included in the article/Supplementary Material, further inquiries can be directed to the corresponding author.

Conflicts of Interest: The authors declare no conflict of interest.

References

1. Babadi, A.A.; Rahmati, S.; Fakhlaei, R.; Barati, B.; Wang, S.; Doherty, W.; Ostrikov, K. Emerging technologies for biodiesel production: Processes, challenges, and opportunities. *Biomass Bioenergy* **2022**, *163*, 106521. [[CrossRef](#)]
2. Abbass, K.; Qasim, M.Z.; Song, H.; Murshed, M.; Mahmood, H.; Younis, I. A review of the global climate change impacts, adaptation, and sustainable mitigation measures. *Environ. Sci. Pollut. Res.* **2022**, *29*, 42539–42559. [[CrossRef](#)]
3. Yusuff, A.S.; Bhonsle, A.K.; Trivedi, J.; Bangwal, D.P.; Singh, L.P.; Atray, N. Synthesis and characterization of coal fly ash supported zinc oxide catalyst for biodiesel production using used cooking oil as feed. *Renew. Energy* **2021**, *170*, 302–314. [[CrossRef](#)]
4. Vargas, E.M.; Ospina, L.; Neves, M.C.; Tarelho, L.A.C.; Nunes, M.I. Optimization of FAME production from blends of waste cooking oil and refined palm oil using biomass fly ash as a catalyst. *Renew. Energy* **2021**, *163*, 1637–1647. [[CrossRef](#)]
5. Bhatia, S.K.; Bhatia, R.K.; Yang, Y.-H. An overview of microdiesel—A sustainable future source of renewable energy. *Renew. Sustain. Energy Rev.* **2017**, *79*, 1078–1090. [[CrossRef](#)]
6. Musthafa, M.M.; Kumar, T.A.; Mohanraj, T.; Chandramouli, R. A comparative study on performance, combustion and emission characteristics of diesel engine fuelled by biodiesel blends with and without an additive. *Fuel* **2018**, *225*, 343–348. [[CrossRef](#)]
7. Niju, S.; Janaranjani, A.; Nanthini, R.; Sindhu, P.A.; Balajii, M. Valorization of banana pseudostem as a catalyst for transesterification process and its optimization studies. *Biomass Convers. Biorefin.* **2023**, *13*, 1805–1818. [[CrossRef](#)]
8. Yameen, M.Z.; Naqvi, S.R.; AlMohamadi, H.; Wang, S. Process optimization, kinetic, and thermodynamic studies of biodiesel production using KOH-modified bio-carbon catalyst derived from marine macroalgae. *Carbon Lett.* **2023**, *33*, 1571–1590. [[CrossRef](#)]
9. Manaf, I.S.A.; Embong, N.H.; Khazaai, S.N.M.; Rahim, M.H.A.; Yusoff, M.M.; Lee, K.T.; Maniam, G.P. A review for key challenges of the development of biodiesel industry. *Energy Convers. Manag.* **2019**, *185*, 508–517. [[CrossRef](#)]
10. Akram, F.; Haq, I.U.; Raja, S.I.; Mir, A.S.; Qureshi, S.S.; Aqeel, A.; Shah, F.I. Current trends in biodiesel production technologies and future progressions: A possible displacement of the petro-diesel. *J. Clean. Prod.* **2022**, *370*, 133479. [[CrossRef](#)]
11. Muratori, M.; Khesghi, H.; Mignone, B.; Clarke, L.; McJeon, H.; Edmonds, J. Carbon capture and storage across fuels and sectors in energy system transformation pathways. *Int. J. Greenh. Gas Control* **2017**, *57*, 34–41. [[CrossRef](#)]
12. Leblanc, F.; Bibas, R.; Mima, S.; Muratori, M.; Sakamoto, S.; Sano, F.; Bauer, N.; Daioglou, V.; Fujimori, S.; Gidden, M.J.; et al. The contribution of bioenergy to the decarbonization of transport: A multi-model assessment. *Clim. Chang.* **2022**, *170*, 21. [[CrossRef](#)]
13. Alsultan, A.G.; Asikin-mijan, N.; Ibrahim, Z.; Yunus, R.; Razali, S.Z.; Mansir, N.; Islam, A.; Seenivasagam, S.; Taufiq-yap, Y.H. A Short Review on Catalyst, Feedstock, Modernised Process, Current State and Challenges on Biodiesel Production. *Catalysts* **2021**, *11*, 1261. [[CrossRef](#)]

14. Bhutto, A.W.; Qureshi, K.; Abro, R.; Harijan, K.; Zhao, Z.; Bazmi, A.A.; Abbas, T.; Yu, G. Progress in the production of biomass-to-liquid biofuels to decarbonize the transport sector-prospects and challenges. *RSC Adv.* **2016**, *6*, 32140–32170. [[CrossRef](#)]
15. Hannula, I.; Reiner, D.M. Near-Term Potential of Biofuels, Electrofuels, and Battery Electric Vehicles in Decarbonizing Road Transport. *Joule* **2019**, *3*, 2390–2402. [[CrossRef](#)]
16. Mukhtar, A.; Saqib, S.; Lin, H.; Hassan Shah, M.U.; Ullah, S.; Younas, M.; Rezakazemi, M.; Ibrahim, M.; Mahmood, A.; Asif, S.; et al. Current status and challenges in the heterogeneous catalysis for biodiesel production. *Renew. Sustain. Energy Rev.* **2022**, *157*, 112012. [[CrossRef](#)]
17. Rezania, S.; Oryani, B.; Park, J.; Hashemi, B.; Yadav, K.K.; Kwon, E.E.; Hur, J.; Cho, J. Review on transesterification of non-edible sources for biodiesel production with a focus on economic aspects, fuel properties and by-product applications. *Energy Convers. Manag.* **2019**, *201*, 112155. [[CrossRef](#)]
18. Don, T.; Sinks, D.; Other, O.R. COOKING OIL Used Cooking Oil Recycling. *Processes* **2013**, *8*, 1–13.
19. Hosseinzadeh-Bandbafha, H.; Nizami, A.-S.; Kalogirou, S.A.; Gupta, V.K.; Park, Y.-K.; Fallahi, A.; Sulaiman, A.; Ranjbari, M.; Rahnama, H.; Aghbashlo, M.; et al. Environmental life cycle assessment of biodiesel production from waste cooking oil: A systematic review. *Renew. Sustain. Energy Rev.* **2022**, *161*, 112411. [[CrossRef](#)]
20. Adekunle, A.S.; Oyekunle, J.A.O.; Oduwale, A.I.; Owootomo, Y.; Obisesan, O.R.; Elugoke, S.E.; Durodola, S.S.; Akintunde, S.B.; Oluwafemi, O.S. Biodiesel potential of used vegetable oils transesterified with biological catalysts. *Energy Rep.* **2020**, *6*, 2861–2871. [[CrossRef](#)]
21. Hsiao, M.C.; Liao, P.H.; Lan, N.V.; Hou, S.S. Enhancement of biodiesel production from high-acid-value waste cooking oil via a microwave reactor using a homogeneous alkaline catalyst. *Energies* **2021**, *14*, 437. [[CrossRef](#)]
22. Hussain, F.; Alshahrani, S.; Abbas, M.M.; Khan, H.M.; Jamil, A.; Yaqoob, H.; Soudagar, M.E.M.; Imran, M.; Ahmad, M.; Munir, M. Review waste animal bones as catalysts for biodiesel production; a mini review. *Catalysts* **2021**, *11*, 630. [[CrossRef](#)]
23. Nguyen, H.C.; Nguyen, M.L.; Su, C.H.; Ong, H.C.; Juan, H.Y.; Wu, S.J. Bio-derived catalysts: A current trend of catalysts used in biodiesel production. *Catalysts* **2021**, *11*, 812. [[CrossRef](#)]
24. Lee, H.; Wu, W.H.; Chen, B.H.; Liao, J.D. Heterogeneous catalysts using strontium oxide agglomerates depositing upon titanium plate for enhancing biodiesel production. *Catalysts* **2021**, *11*, 30. [[CrossRef](#)]
25. Gebremariam, S.N.; Marchetti, J.M. Biodiesel production process using solid acid catalyst: Influence of market variables on the process's economic feasibility. *Biofuels Bioprod. Biorefin.* **2021**, *15*, 815–824. [[CrossRef](#)]
26. Banurea, I.R.; Setyawan, N.; Yuliani, S.; Herawati, H.; Hoerudin. Utilization of rice husk silica as solid catalyst in the transesterification process for biodiesel production. *IOP Conf. Ser. Earth Environ. Sci.* **2021**, *739*, 012083. [[CrossRef](#)]
27. Sadeek, S.A.; Mohammed, E.A.; Shaban, M.; Abou Kana, M.T.H.; Negm, N.A. Synthesis, characterization and catalytic performances of activated carbon-doped transition metals during biofuel production from waste cooking oils. *J. Mol. Liq.* **2020**, *306*, 112749. [[CrossRef](#)]
28. Khan, W.U.H.; Khoja, A.H.; Gohar, H.; Naqvi, S.R.; Din, I.U.; Lumbers, B.; Salem, M.A.; Alzahrani, A.Y. In depth thermokinetic investigation on Co-pyrolysis of low-rank coal and algae consortium blends over CeO₂ loaded hydrotalcite (MgNiAl) catalyst. *J. Environ. Chem. Eng.* **2022**, *10*, 108293. [[CrossRef](#)]
29. Hossain, N.; Bhuiyan, M.A.; Pramanik, B.K.; Nizamuddin, S.; Griffin, G. Waste materials for wastewater treatment and waste adsorbents for biofuel and cement supplement applications: A critical review. *J. Clean. Prod.* **2020**, *255*, 120261. [[CrossRef](#)]
30. Hossain, N.; Nizamuddin, S.; Griffin, G.; Selvakannan, P.; Mubarak, N.M.; Mahlia, T.M.I. Synthesis and characterization of rice husk biochar via hydrothermal carbonization for wastewater treatment and biofuel production. *Sci. Rep.* **2020**, *10*, 18851. [[CrossRef](#)]
31. Macdermid-Watts, K.; Adewakun, E.; Norouzi, O.; Abhi, T.D.; Pradhan, R.; Dutta, A. Effects of FeCl₃ Catalytic Hydrothermal Carbonization on Chemical Activation of Corn Wet Distillers' Fiber. *ACS Omega* **2021**, *6*, 14875–14886. [[CrossRef](#)]
32. Naji, S.Z.; Tye, C.T. A review of the synthesis of activated carbon for biodiesel production: Precursor, preparation, and modification. *Energy Convers. Manag. X* **2022**, *13*, 100152. [[CrossRef](#)]
33. Omar, R.; Robinson, J.P. Conventional and microwave-assisted pyrolysis of rapeseed oil for bio-fuel production. *J. Anal. Appl. Pyrolysis* **2014**, *105*, 131–142. [[CrossRef](#)]
34. Yigezu, Z.D.; Muthukumar, K. Catalytic cracking of vegetable oil with metal oxides for biofuel production. *Energy Convers. Manag.* **2014**, *84*, 326–333. [[CrossRef](#)]
35. Koide, T.; Aritome, I.; Saeki, T.; Morita, Y.; Shiota, Y.; Yoshizawa, K.; Shimakoshi, H.; Hisaeda, Y. Cobalt-Carbon Bond Formation Reaction via Ligand Reduction of Porphycene-Cobalt(II) Complex and Its Noninnocent Reactivity. *ACS Omega* **2018**, *3*, 4027–4034. [[CrossRef](#)] [[PubMed](#)]
36. Thangadurai, T.; Tye, C.T. Performance of activated carbon supported cobalt oxides and iron oxide catalysts in catalytic cracking of waste cooking oil. *Period. Polytech. Chem. Eng.* **2021**, *65*, 350–360. [[CrossRef](#)]
37. Mustafa, A.; Faisal, S.; Ahmed, I.A.; Munir, M.; Cipolatti, E.P.; Manoel, E.A.; Pastore, C.; di Bitonto, L.; Hanelt, D.; Nitbani, F.O.; et al. Has the time finally come for green oleochemicals and biodiesel production using large-scale enzyme technologies? Current status and new developments. *Biotechnol. Adv.* **2023**, *69*, 108275. [[CrossRef](#)]
38. Mustafa, A.; Ramadan, R.; Niikura, F.; Inayat, A.; Hafez, H. Highly selective synthesis of glyceryl monostearate via lipase catalyzed esterification of triple pressed stearic acid and glycerin. *Sustain. Energy Technol. Assess.* **2023**, *57*, 103200. [[CrossRef](#)]

39. Selvaraj, R.; Moorthy, I.G.; Kumar, R.V.; Sivasubramanian, V. Microwave mediated production of FAME from waste cooking oil: Modelling and optimization of process parameters by RSM and ANN approach. *Fuel* **2019**, *237*, 40–49. [[CrossRef](#)]
40. Manojkumar, N.; Muthukumaran, C.; Sharmila, G. A comprehensive review on the application of response surface methodology for optimization of biodiesel production using different oil sources. *J. King Saud Univ.—Eng. Sci.* **2022**, *34*, 198–208. [[CrossRef](#)]
41. Yahya, M.D.; Obayomi, K.S.; Abdulkadir, M.B.; Iyaka, Y.A.; Olugbenga, A.G. Characterization of cobalt ferrite-supported activated carbon for removal of chromium and lead ions from tannery wastewater via adsorption equilibrium. *Water Sci. Eng.* **2020**, *13*, 202–213. [[CrossRef](#)]
42. Puccini, M.; Ceccarini, L.; Antichi, D.; Seggiani, M.; Tavarini, S.; Hernandez Latorre, M.; Vitolo, S. Hydrothermal Carbonization of Municipal Woody and Herbaceous Prunings: Hydrochar Valorisation as Soil Amendment and Growth Medium for Horticulture. *Sustainability* **2018**, *10*, 846. [[CrossRef](#)]
43. Khan, M.; Farah, H.; Iqbal, N.; Noor, T.; Amjad, M.Z.B.; Ejaz Bukhari, S.S. A TiO₂ composite with graphitic carbon nitride as a photocatalyst for biodiesel production from waste cooking oil. *RSC Adv.* **2021**, *11*, 37575–37583. [[CrossRef](#)] [[PubMed](#)]
44. Jamil, U.; Husain Khoja, A.; Liaquat, R.; Raza Naqvi, S.; Nor Nadyaini Wan Omar, W.; Aishah Saidina Amin, N. Copper and calcium-based metal organic framework (MOF) catalyst for biodiesel production from waste cooking oil: A process optimization study. *Energy Convers. Manag.* **2020**, *215*, 112934. [[CrossRef](#)]
45. ASTM D6751-20a; Standard Specification for Biodiesel Fuel Blend Stock (B100) for Middle Distillate Fuels. ASTM International: West Conshohocken, PA, USA, 2020. [[CrossRef](#)]
46. Soltani, H.; Karimi, A.; Falahatpisheh, S. The optimization of biodiesel production from transesterification of sesame oil via applying ultrasound-assisted techniques: Comparison of RSM and ANN-PSO hybrid model. *Chem. Prod. Process Model.* **2022**, *17*, 55–67. [[CrossRef](#)]
47. Özgür, C. Optimization of biodiesel yield and diesel engine performance from waste cooking oil by response surface method (RSM). *Pet. Sci. Technol.* **2021**, *39*, 683–703. [[CrossRef](#)]
48. Li, L.; Zhang, Y.; Yang, S.; Zhang, S.; Xu, Q.; Chen, P.; Du, Y.; Xing, Y. Cobalt-loaded cherry core biochar composite as an effective heterogeneous persulfate catalyst for bisphenol A degradation. *RSC Adv.* **2022**, *12*, 7284–7294. [[CrossRef](#)]
49. Wang, M.; Cui, Y.; Cao, H.; Wei, P.; Chen, C.; Li, X.; Xu, J.; Sheng, G. Activating peroxydisulfate with Co₃O₄/NiCo₂O₄ double-shelled nanocages to selectively degrade bisphenol A—A nonradical oxidation process. *Appl. Catal. B Environ.* **2021**, *282*, 119585. [[CrossRef](#)]
50. Omri Abdessalem, B.M. Characterization of Activated Carbon Prepared From a New Raw Lignocellulosic Material: Ziziphus Spina-Christi Seeds. *J. Soc. Chim. Tunis.* **2012**, *14*, 175–183.
51. Saad, M.J.; Chia, C.H.; Zakaria, S.; Sajab, M.S.; Misran, S.; Rahman, M.H.A.; Chin, S.X. Physical and chemical properties of the rice straw activated carbon produced from carbonization and KOH activation processes. *Sains Malays.* **2019**, *48*, 385–391. [[CrossRef](#)]
52. bin Tang, Y.; Liu, Q.; yan Chen, F. Preparation and characterization of activated carbon from waste ramulus mori. *Chem. Eng. J.* **2012**, *203*, 19–24. [[CrossRef](#)]
53. Sreńscek-Nazzal, J.; Kamińska, W.; Michalkiewicz, B.; Koren, Z.C. Production, characterization and methane storage potential of KOH-activated carbon from sugarcane molasses. *Ind. Crops Prod.* **2013**, *47*, 153–159. [[CrossRef](#)]
54. Shukla, P.R.; Wang, S.; Sun, H.; Ang, H.M.; Tadé, M. Activated carbon supported cobalt catalysts for advanced oxidation of organic contaminants in aqueous solution. *Appl. Catal. B Environ.* **2010**, *100*, 529–534. [[CrossRef](#)]
55. Shen, Y.; Fu, Y. KOH-activated rice husk char via CO₂ pyrolysis for phenol adsorption. *Mater. Today Energy* **2018**, *9*, 397–405. [[CrossRef](#)]
56. Scapin, E.; Maciel, G.P.d.S.; Polidoro, A.D.S.; Lazzari, E.; Benvenuti, E.V.; Falcade, T.; Jacques, R.A. Activated carbon from rice husk biochar with high surface area. *Biointerface Res. Appl. Chem.* **2021**, *11*, 10265–10277. [[CrossRef](#)]
57. Izhah, I.; Amin, N.A.S.; Asmadi, M. Dry reforming of methane over oil palm shell activated carbon and ZSM-5 supported cobalt catalysts. *Int. J. Green Energy* **2017**, *14*, 831–838. [[CrossRef](#)]
58. Das, V.; Tripathi, A.M.; Borah, M.J.; Dunford, N.T.; Deka, D. Cobalt-doped CaO catalyst synthesized and applied for algal biodiesel production. *Renew. Energy* **2020**, *161*, 1110–1119. [[CrossRef](#)]
59. Mendonça, I.M.; Paes, O.A.R.L.; Maia, P.J.S.; Souza, M.P.; Almeida, R.A.; Silva, C.C.; Duvoisin, S.; de Freitas, F.A. New heterogeneous catalyst for biodiesel production from waste tucumã peels (*Astrocaryum aculeatum* Meyer): Parameters optimization study. *Renew. Energy* **2019**, *130*, 103–110. [[CrossRef](#)]
60. Miladinović, M.R.; Zdujić, M.V.; Veljović, D.N.; Krstić, J.B.; Banković-Ilić, I.B.; Veljković, V.B.; Stamenković, O.S. Valorization of walnut shell ash as a catalyst for biodiesel production. *Renew. Energy* **2020**, *147*, 1033–1043. [[CrossRef](#)]
61. Nath, B.; Kalita, P.; Das, B.; Basumatary, S. Highly efficient renewable heterogeneous base catalyst derived from waste Sesamum indicum plant for synthesis of biodiesel. *Renew. Energy* **2020**, *151*, 295–310. [[CrossRef](#)]
62. Imamoglu, M.; Tekir, O. Removal of copper (II) and lead (II) ions from aqueous solutions by adsorption on activated carbon from a new precursor hazelnut husks. *Desalination* **2008**, *228*, 108–113. [[CrossRef](#)]
63. Guo, F.; Peng, Z.G.; Dai, J.Y.; Xiu, Z.L. Calcined sodium silicate as solid base catalyst for biodiesel production. *Fuel Process. Technol.* **2010**, *91*, 322–328. [[CrossRef](#)]
64. Ismail, S.; Abu, S.A.; Rezaur, R.; Sinin, H. Biodiesel Production from Castor Oil and Its Application in Diesel Engine. *ASEAN J. Sci. Technol. Dev.* **2014**, *31*, 90–100. [[CrossRef](#)]

65. Moazeni, F.; Chen, Y.C.; Zhang, G. Enzymatic transesterification for biodiesel production from used cooking oil, a review. *J. Clean. Prod.* **2019**, *216*, 117–128. [[CrossRef](#)]
66. Ayetor, G.K.; Sunnu, A.; Parbey, J. Effect of biodiesel production parameters on viscosity and yield of methyl esters: *Jatropha curcas*, *Elaeis guineensis* and *Cocos nucifera*. *Alex. Eng. J.* **2015**, *54*, 1285–1290. [[CrossRef](#)]
67. ASTM D6751-02-2002; Standard Specification for Biodiesel Fuel (B100) Blend Stock for Distillate Fuels. ASTM International: West Conshohocken, PA, USA, 2002.
68. Gao, Z.; Ma, Y.; Ma, X.; Wang, Q.; Liu, Y. A novel variable pH control strategy for enhancing lipid production from food waste: Biodiesel versus docosahexaenoic acid. *Energy Convers. Manag.* **2019**, *189*, 60–66. [[CrossRef](#)]
69. Remón, J.; Ruiz, J.; Oliva, M.; García, L.; Arauzo, J. Effect of biodiesel-derived impurities (acetic acid, methanol and potassium hydroxide) on the aqueous phase reforming of glycerol. *Chem. Eng. J.* **2016**, *299*, 431–448. [[CrossRef](#)]
70. Drenth, A.C.; Olsen, D.B.; Deneff, K. Fuel property quantification of triglyceride blends with an emphasis on industrial oilseeds camelina, carinata, and pennycress. *Fuel* **2015**, *153*, 19–30. [[CrossRef](#)]
71. Drenth, A.C.; Olsen, D.B.; Cabot, P.E.; Johnson, J.J. Compression ignition engine performance and emission evaluation of industrial oilseed biofuel feedstocks camelina, carinata, and pennycress across three fuel pathways. *Fuel* **2014**, *136*, 143–155. [[CrossRef](#)]
72. Tang, Z.E.; Lim, S.; Pang, Y.L.; Ong, H.C.; Lee, K.T. Synthesis of biomass as heterogeneous catalyst for application in biodiesel production: State of the art and fundamental review. *Renew. Sustain. Energy Rev.* **2018**, *92*, 235–253. [[CrossRef](#)]
73. Bayat, A.; Baghdadi, M.; Bidhendi, G.N. Tailored magnetic nano-alumina as an efficient catalyst for transesterification of waste cooking oil: Optimization of biodiesel production using response surface methodology. *Energy Convers. Manag.* **2018**, *177*, 395–405. [[CrossRef](#)]
74. Nisar, J.; Razaq, R.; Farooq, M.; Iqbal, M.; Khan, R.A.; Sayed, M.; Shah, A.; Rahman, I. Enhanced biodiesel production from *Jatropha* oil using calcined waste animal bones as catalyst. *Renew. Energy* **2017**, *101*, 111–119. [[CrossRef](#)]
75. Enweremadu, C.C.; Rutto, H.L. Optimization and modeling of process variables of biodiesel production from Marula oil using response surface methodology. *J. Chem. Soc. Pak.* **2015**, *37*, 256–265. [[CrossRef](#)]
76. Moyo, L.B.; Iyuke, S.E.; Muvhiiwa, R.F.; Simate, G.S.; Hlabangana, N. Application of response surface methodology for optimization of biodiesel production parameters from waste cooking oil using a membrane reactor. *S. Afr. J. Chem. Eng.* **2021**, *35*, 1–7. [[CrossRef](#)]
77. Ngadi, N.; Ma, L.N.; Alias, H.; Johari, A.; Rahman, R.A.; Mohamad, M. Production of Biodiesel from Waste Cooking Oil via Ultrasonic-Assisted Catalytic System. *Appl. Mech. Mater.* **2014**, *699*, 552–557. [[CrossRef](#)]
78. Razzaq, L.; Abbas, M.M.; Miran, S.; Asghar, S.; Nawaz, S.; Soudagar, M.E.M.; Shaukat, N.; Veza, I.; Khalil, S.; Abdelrahman, A.; et al. Response Surface Methodology and Artificial Neural Networks-Based Yield Optimization of Biodiesel Sourced from Mixture of Palm and Cotton Seed Oil. *Sustainability* **2022**, *14*, 6130. [[CrossRef](#)]
79. Mohamed, R.M.; Kadry, G.A.; Abdel-Samad, H.A.; Awad, M.E. High operative heterogeneous catalyst in biodiesel production from waste cooking oil. *Egypt. J. Pet.* **2020**, *29*, 59–65. [[CrossRef](#)]
80. Borah, M.J.; Devi, A.; Borah, R.; Deka, D. Synthesis and application of Co doped ZnO as heterogeneous nanocatalyst for biodiesel production from non-edible oil. *Renew. Energy* **2019**, *133*, 512–519. [[CrossRef](#)]
81. Gutiérrez-Ortega, N.; Ramos-Ramírez, E.; Serafín-Muñoz, A.; Zamorategui-Molina, A.; Monjaraz-Vallejo, J. Use of Co/Fe-Mixed oxides as heterogeneous catalysts in obtaining biodiesel. *Catalysts* **2019**, *9*, 403. [[CrossRef](#)]
82. Li, E.; Xu, Z.P.; Rudolph, V. MgCoAl-LDH derived heterogeneous catalysts for the ethanol transesterification of canola oil to biodiesel. *Appl. Catal. B Environ.* **2009**, *88*, 42–49. [[CrossRef](#)]
83. Singh, S.; Mukherjee, D.; Dinda, S.; Ghosal, S.; Chakrabarty, J. Synthesis of CoO–NiO promoted sulfated ZrO₂ super-acid oleophilic catalyst via co-precipitation impregnation route for biodiesel production. *Renew. Energy* **2020**, *158*, 656–667. [[CrossRef](#)]

Disclaimer/Publisher’s Note: The statements, opinions and data contained in all publications are solely those of the individual author(s) and contributor(s) and not of MDPI and/or the editor(s). MDPI and/or the editor(s) disclaim responsibility for any injury to people or property resulting from any ideas, methods, instructions or products referred to in the content.